ISSN 0021-3640, JETP Letters, 2013, Vol. 98, No. 5, pp. 278–284. © Pleiades Publishing, Ltd., 2013.
Original Russian Text © Yu.V. Petrov, N.A. Inogamov, 2013, published in Pis'ma v Zhurnal Eksperimental'noi i Teoreticheskoi Fiziki, 2013, Vol. 98, No. 5, pp. 316–322.

Elimination of the Mott Interband *s*–*d* Enhancement of the Electrical Resistance of Nickel and Platinum Owing to the Excitation of Electrons by Femtosecond Laser Pulses

Yu. V. Petrov and N. A. Inogamov

Landau Institute for Theoretical Physics, Russian Academy of Sciences, Chernogolovka, Moscow region, 142432 Russia
e-mail: nailinogamov@googlemail.com

Received July 19, 2013

The dependence of electrical, σ, and thermal, κ, conductivities of metals on the electron temperature T_e at high (~1 eV) T_e values has been calculated. The two-temperature states for which the temperature T_e of heated electrons exceeds the temperature T_i of ions in the crystal lattice result from the excitation of electrons by femtosecond laser pulses. It is well known that the existence of empty *d* levels with a high density of states near the Fermi surface (as, e.g., in nickel, platinum, and iron) leads to a pronounced enhancement of the electrical resistance (Mott, 1936). This is due to an increase in the statistical factor related to the electron transitions to the empty states induced by collisions with phonons. It is found that the excitation of the electron subsystem significantly reduces the electron–phonon scattering to unoccupied *d* states since the chemical potential $\mu(T_e)$ rises above the upper edge of the *d* band. The decrease in the scattering probability leads to the anomalous behavior of the conductivity σ_{el-ph}, which *increases* with the temperature T_e. Such a behavior turns out to be inverse with respect to the usual situation in condensed matter.

DOI: 10.1134/S0021364013180094

Femtosecond laser pulses are used in numerous modern technologies: modifications of optical, hydrophobic, catalytic, etc., characteristics of surfaces owing to nanostructuring or plastic modification; enhancement of the hardness owing to laser-induced pinning; sputtering film deposition; keratotomy in ophthalmology; nanoplasmonics; nanophotonics; metaoptics; printing by the laser-induced transfer of small portions of different films from one surface to another (LIFT); etc. The material processing in the aforementioned techniques is based on a pronounced increase in temperature and in dynamic stresses during a very short time within a very thin (about 10–10^3 nm) surface layer of a solid heated owing to thermal conductivity. Here, the absorption of laser energy is accompanied by the onset of the two-temperature stage, at which the thermal energy of excited electrons far exceeds that of the lattice [1].

The numerical simulation of the thermal and dynamical phenomena in metals starts from the calculations of the thermal conductivity κ since the κ value at the two-temperature stage ($T_e \gg T_i$) exceeds by a factor of 10–30 the corresponding single-temperature values and is determined with an insufficient accuracy. Because of such high κ values, the thickness of the heated layer ($d_T \sim 100$ nm) far exceeds the skin layer thickness (about 15 nm), in which radiation is absorbed. The thermal scale d_T grows with κ. Along with the scale d_T, the melting and ablation thresholds increase (of course, at the fixed parameters characterizing the electron–ion heat transfer, latent heat of fusion, and dynamic strength within the range of deformation rates under study).

The thermal conductivity κ is determined by the collision rates of heat carriers (electrons) with ions (ν_{ei}) and with other electrons (ν_{ee}) The contribution of ν_{ee} becomes appreciable at high values of T_e when the electron degeneracy is partially lifted. At room temperature, the contribution coming from ν_{ee} can be neglected in comparison to that of ν_{ei}. The contribution of ν_{ee} was explicitly calculated earlier for single-band metals [2] and for two-band metals [3]. The calculations reported in [2, 3] involved the matrix elements for the scattering amplitude and the kinetic equation.

The total frequency ν is determined as a sum

$$\nu = \nu_{ei} + \nu_{ee}. \quad (1)$$

As we mentioned above, the ν_{ee} term in sum (1) can be explicitly calculated [2, 3].It is usually assumed that the ν_{ei} term depends only on the ion temperature T_i [2–7].

In addition, the dependence of ν_{ei} on the temperature T_i is usually taken from experimental data. The simplest approximation for ν_{ei} linear in temperature T_i is often used [4–7]. It is well known that, above the Debye temperature, the electron–phonon collision rate increases almost linearly with the temperature,

since the amplitude squared of thermal ionic vibrations is a linearly increasing function of the temperature. A more accurate approach takes into account the kink at the Curie point (if such a point exists) along with the melting and saturation at the minimum value of metallic conductivity (about 1 μΩ m) [2, 3]. If the experimental data are used, the ion temperature T_i in the two-temperature situation is assumed to coincide with the temperature T corresponding to the single-temperature case, $T = T_i = T_e$. Of course, the $T_i \longrightarrow T$ substitution is based on the assumption that the frequency ν_{ei} is independent of the temperature T_e.

Let us discuss the implications of the assumption that the frequency ν_{ei} depends only on T_i and is independent of T_e,

$$\nu_{ei}(T_e, T_i) \approx \nu_{ei}(T_i). \quad (2)$$

At the two-temperature stage, the heat wave moves to the target bulk at supersonic speed. Therefore, at this stage, in the main volume of the heated layer, the density of the material is approximately equal to the initial density (isochoric process). Thus, we neglect the dependence on density. Only the temperature dependence remains. The mean free time $1/\nu_{ei}$ between the electron–ion scattering acts depends on the electron velocity v_e and on the cross section for scattering by the ion subsystem. Within the electron temperature range of the order of several electronvolts, velocity v_e is slightly growing in comparison to the Fermi velocity v_F. Within approximation (2), this dependence is usually disregarded, $v_e(T_e) \approx v_F$.

In addition, it is usually assumed that the cross section for scattering by ions depends only on the degree of ordering in the ion subsystem. In the ideal system, this cross section vanishes. It is often argued that the degree of ordering is mainly determined by the ion temperature T_i. This results in approximation (2). Of course, the statement that the ordering is determined only by the value of T_i implies neglecting the dependence of elastic constants on the temperature T_e. The dependence of the other parameters on the temperature T_e is important in semiconductors [8] and insulators [9]. This is the basis of the popular mechanism underlying the superfast nonthermal melting due to the lowering of rigidity and the acoustic instability of the crystal lattice arising at the excitation (ionization) of electrons from the valence band to the conduction band [10].

In metals, we deal with the electron excitations within the conduction bands. The elastic constants in a metal can both be insensitive to the electron excitations (e.g., in aluminum [8, 11]) and be enhanced with the growth of the temperature T_e (e.g., in gold [8]). The enhancement of rigidity in gold with T_e [8, 12] is rather moderate. Indeed, the shift of the melting point due to the growth of T_e (the shift of the melting curve $T_m(p, T_e)$) is not large if this shift is normalized with

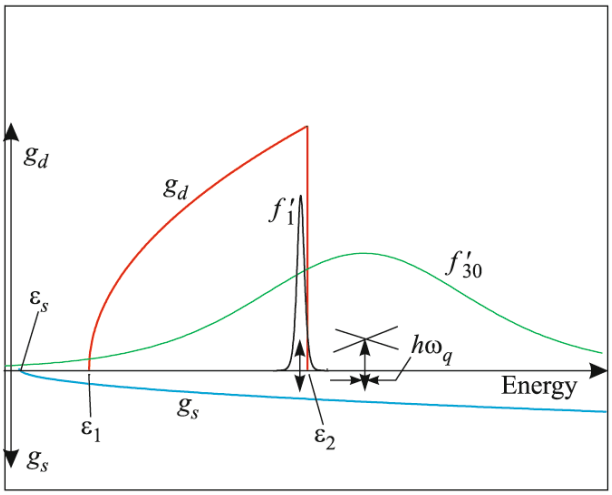

Fig. 1. Enhancement of the electrical resistance of transition metals at moderate temperatures T_e is caused by an increase in the statistical factor [13, 14] involved in the scattering probability. In transition metals, the statistical factor is large in comparison to that in the metals with the single-band conductivity. The statistical factor grows owing to the high density of empty *d* states. When the chemical potential attains the upper edge of the *d* band ε_2 and exceeds it, the statistical factor decreases (no transitions to the *d* band occur; the upper head of the right double-headed arrow is crossed). The double-headed arrows are placed at the points corresponding to the chemical potential $\mu(T_e = 1\ \text{kK}) \approx 0 < \varepsilon_2$ and $\mu(T_e = 30\ \text{kK}) \approx +2.3\ \text{eV} > \varepsilon_2$. The values of ε_s, ε_1, and ε_2 calculated for platinum in the framework of the density functional theory are −10, −7.5, and +0.27 eV, respectively.

respect to the value of the single-temperature melting point at a given pressure, $[T_m(p, T_e) - T_m(p])/T_m(p)$. We neglect a small lowering of the electrical resistance due to the increase in rigidity and the speed of sound with temperature T_e in gold.

We refer to the effect described in seminal papers [13, 14] as the Mott effect (see Fig. 1). The Mott effect leads to a pronounced enhancement of electrical resistivity in metals with a partially filled *d* band. There are a lot of such metals. Nickel, platinum, iron, titanium, tungsten, tantalum, and other metals have a partially filled *d* band. The larger the density of states $g_d(\varepsilon_F)$ in the *d* band near the Fermi surface, the stronger is the effect. Nickel and platinum have record values of $g_d(\varepsilon_F)$. The decrease in the electron mean free path lowers the electrical and thermal conductivities. The increase in the scattering cross section is caused by the electron scattering to the unoccupied states at collisions with phonons (Fig. 1).

The calculations of the electron–phonon interaction in metals discussed in this paper demonstrate that relation (2) is indeed approximately met in the metals that do not exhibit the Mott effect. It turns out that the increase in the *e–i* scattering cross section does not manifest itself in the transition metals at high electron

temperatures. Therefore, the frequency ν_{ei} in the transition metals depends on both T_i and T_e in contrast to assumption (2).

We illustrate this consideration in Fig. 1. For better visualization, $g_s(\varepsilon)$ and $g_d(\varepsilon)$ curves corresponding to the energy dependence of the electron density of states for the *s* and *d* conduction bands are plotted along the upward and downward vertical axes. A parabolic approximation is used for the approximate description of the density of states determined by the quantum-mechanical calculations for the electron subsystem in the crystal [3]. It is important that, in transition metals at room temperature, the *d* band edge ε_2 is located to the right of the Fermi level $\mu(T_e = 0)$. That is why the electron transitions to the unoccupied *d* states are possible with the emission or absorption of a phonon. The functions f_1' and f_{30}' plotted in Fig. 1 are the derivatives of the Fermi distribution $f = [1 - e^{(\varepsilon-\mu)/k_B T_e}]^{-1}$ with respect to ε taken with the opposite sign at $T_e = 1$ and 30 kK, respectively. In Fig. 1, the scales for the plots of the functions f_1' and f_{30}' are different. They are chosen in such a way that the heights of the plots become comparable to each other. It is well known that the charge and heat transfer involves the electrons falling within the range corresponding to appreciable values of derivative f' (see expression (12) below). The occupied and empty states are located to the left and right of this range, respectively.

The maximum value of derivative f' corresponds to the point where $\varepsilon = \mu$. In Fig. 1, the points of maximum are indicated by the double-headed arrows. The left double-headed arrow denotes the transitions to the empty *d* states. In this case, the statistical factor is large since the density of *d* states is quite high and the energy range including the f_1' function is situated within the *d* band (i.e., to the left of the upper edge ε_2 of the *d* band). In the case corresponding to the right double-headed arrow, most of the *s* electrons cannot come to the *d* band because, first, the electron–ion interaction is quasielastic and, second, the main part of the range covered by f_{30}' is located *to the right* of the *d* band edge. Therefore, the upper head of the right double-headed arrow is marked by a cross. In the case of f_{30}', the statistical factor is substantially reduced in comparison to that for f_1'. It is important that, in the transition metals (with small positive values of the difference $\varepsilon_2 - \mu(0)$), the chemical potential $\mu(T_e)$ undergoes quite an appreciable shift toward larger energies with the growth of the temperature T_e. Thus, the f_{30}' function is shifted with respect to the *d* band. The width of the $\hbar\omega_q$ range that characterizes the change in the electron energy in the *e–i* interaction is small in comparison to the characteristic scales of the electron energies (quasielastic case). In Fig. 1, this range is indicated by arrows with the legend $\hbar\omega_q$.

Let us now go from the qualitative explanations to the calculations of the frequency $\nu_{ei}(T_e, T_i)$ in the two-temperature situation, $T_e > T_i$. We approximate the electron spectrum by two parabolas (see Fig. 1 and [3]),

$$\varepsilon(\mathbf{p}) = \varepsilon_s + p^2/2m_s, \quad \varepsilon(\mathbf{p}') = \varepsilon_1 + p'^2/2m_d, \qquad (3)$$

corresponding to the *s* and *d* bands with the effective masses m_s and m_d, respectively (e.g., $4s^2 3d^8$ or $4s^1 3d^9$ in Ni and $6s^1 5d^9$ in Pt). The parameters of the parabolas are determined from the density functional simulation of the quantum state of the crystal [3]. The electron distribution functions for the *s* and *d* bands, $f_s(\mathbf{p}) = [1 + e^{(\varepsilon_s-\mu)/k_B T_e}]^{-1}$ and $f_d(\mathbf{p}') = [1 + e^{(\varepsilon_d-\mu)/k_B T_e}]^{-1}$, have common values of the chemical potential $\mu(T_e)$ and of the temperature. The energy of *d* electrons in Eqs. (3) falls within the *d* band $\varepsilon_1 \le \varepsilon(\mathbf{p}') \le \varepsilon_2$ (see Fig. 1 and [3]). The band edges are shown in Fig. 1. The phonons are described by the distribution function $N(\mathbf{q}) = [e^{\hbar\omega_\mathbf{q}/k_B T_i} - 1]^{-1}$, which depends on the momentum $\mathbf{q}$ of a phonon and on the temperature.

The number of *s* electrons leaving an element of the phase volume $d\mathbf{p}/(2\pi\hbar)^3$ per unit time and coming to the *s* band ($s \longrightarrow s$) is equal to

$$f_s(\mathbf{p})\frac{2d\mathbf{p}}{(2\pi\hbar)^3}\int W^{ss}_{\mathbf{pp}'}\delta[1 - f_s(\mathbf{p}')](N_\mathbf{q} + 1)\frac{Vd\mathbf{p}'}{(2\pi\hbar)^3}. \qquad (4)$$

The rate of the decrease in the number of *s* electrons, $\dot{N}_-^{s,\,s+\mathrm{ph}}$ (4), is related to the emission of phonons with the momentum $\mathbf{q}$. This process can be written as $\mathbf{p} = \mathbf{p}' + \mathbf{q}$. In the notation $\dot{N}_-^{s,\,s+\mathrm{ph}}$, the superscript means an *s* electron has emitted a phonon (ph) and remained an *s* electron ($s \longrightarrow s + \mathrm{ph}$). The subscript (here, minus) indicates the decrease in the number of electrons. The subscript "plus" means that the number of electrons increases. Expression (4) implies the quasielasticity of scattering (the phonon energy is low). Therefore, we write $\delta = \delta(\varepsilon - \varepsilon')$ instead of $\delta(\varepsilon - \varepsilon' - \hbar\omega(\mathbf{q}))$.

The formulas for the other cases of changes in the number of particles are represented similarly to Eq. (4):

• $\dot{N}_-^{s+\mathrm{ph},\,s}$ describes electrons coming from the *s* band to the *s* band ($s \longrightarrow s$) from the volume $d\mathbf{p}/(2\pi\hbar)^3$ owing to the absorption of a phonon (process $\mathbf{p} = \mathbf{p}' - \mathbf{q}$). The matrix element $W^{ss}_{\mathbf{pp}'}$ is the same as in Eq. (4).

• $\dot{N}_-^{s,\,d+\mathrm{ph}}$ describes the $s \longrightarrow d$ electrons coming from volume $d\mathbf{p}/(2\pi\hbar)^3$ owing to the emission of a

phonon (process $\mathbf{p} = \mathbf{p}' + \mathbf{q}$). The matrix element has the form $W^{sd}_{\mathbf{pp}'}$.

• $\dot{N}_-^{s+\mathrm{ph},d}$ describes the $s \longrightarrow d$ electrons coming from the volume $d\mathbf{p}/(2\pi\hbar)^3$ owing to the absorption of a phonon (process $\mathbf{p} = \mathbf{p}' - \mathbf{q}$).

• $\dot{N}_+^{s,s+\mathrm{ph}}$ describes the $s \longrightarrow s$ electrons coming from the volume $d\mathbf{p}/(2\pi\hbar)^3$ owing to the emission of a phonon (process $\mathbf{p} = \mathbf{p}' + \mathbf{q}$).

There are three additional contributions $\dot{N}_+^{s+\mathrm{ph},s}$, $\dot{N}_+^{s,d+\mathrm{ph}}$, and $\dot{N}_+^{s+\mathrm{ph},d}$ increasing the number of particles.

Summing four types of coming particles $\dot{N}_+$ and four types of leaving particles $\dot{N}_-$, we arrive at the following expression for the rate $\dot{N}^s$ of change in the number of particles in the volume $d\mathbf{p}/(2\pi\hbar)^3$ in the s band:

$$\dot{N}^s = (S^s + D^s)\cdot 2d\mathbf{p}/(2\pi\hbar)^3,$$

$$S^s = \int_s W^{ss}_{\mathbf{pp}'}\delta[f_s(\mathbf{p}') - f_s(\mathbf{p})](2N_\mathbf{q}+1)\frac{Vd\mathbf{p}'}{(2\pi\hbar)^3}, \quad (5)$$

$$D^s = \int_d W^{sd}_{\mathbf{pp}'}\delta[f_d(\mathbf{p}') - f_s(\mathbf{p})](2N_\mathbf{q}+1)\frac{Vd\mathbf{p}'}{(2\pi\hbar)^3},$$

where again $\delta = \delta(\varepsilon - \varepsilon')$.

Similarly to Eq. (5), the change in the number of d electrons in the volume element $d\mathbf{p}/(2\pi\hbar)^3$ is equal to

$$\dot{N}^d = (D^d + S^d)\cdot 2d\mathbf{p}/(2\pi\hbar)^3. \quad (6)$$

Relations (5) and (6) correspond to the collision terms in the kinetic equation. The left-hand side of the kinetic equation has the form

$$df/dt = \partial f/\partial\mathbf{p}\cdot e\mathbf{E} = f'_\varepsilon\mathbf{v}\cdot e\mathbf{E} = (e/m^*)f'_\varepsilon\mathbf{pE},$$

where $\mathbf{E}$ is the electric field vector, m^* is the effective mass, and $f'_\varepsilon = \partial f/\partial\varepsilon$. In the relaxation time approximation

$$df/dt = -(f - f_0)/\tau(\mathbf{p}) = -f_1(\mathbf{p})/\tau(\mathbf{p}) = (e/m^*)f'_\varepsilon\mathbf{pE},$$

we find the correction $f_1 = (e/m^*)(-f'_\varepsilon)\mathbf{pE}\tau(\mathbf{p})$ to the equilibrium (Fermi) distribution function f_0.

Then, we linearize both kinetic equations with respect to the sought small corrections, f_1^s and f_1^d, to the equilibrium distribution. Owing to the quasi-elasticity of the collisions, $(-f'_\varepsilon) = (-f'_{\varepsilon'})$. Using this relationship, we can write the corrections in the form $f_1^s = \eta_s(\varepsilon)\mathbf{pE}\tau_s(\varepsilon)$ and $f_1^d = \eta_d(\varepsilon)\mathbf{pE}\tau_d(\varepsilon)$. Hence, we obtain the following kinetic equation for s electrons:

$$-\eta_s(\varepsilon)\mathbf{pE} = \int_s W^{ss}_{\mathbf{pp}'}\delta[\eta_s(\varepsilon)\mathbf{p}'\mathbf{E}\tau_s(\varepsilon) - \eta_s(\varepsilon)\mathbf{pE}\tau_s(\varepsilon)]\xi + \int_d W^{sd}_{\mathbf{pp}'}\delta[\eta_d(\varepsilon)\mathbf{p}'\mathbf{E}\tau_d(\varepsilon) - \eta_s(\varepsilon)\mathbf{pE}\tau_s(\varepsilon)]\xi,$$

where $\delta \equiv \delta(\varepsilon - \varepsilon')$ and $\xi = (2N_\mathbf{q}+1)Vd\mathbf{p}'/(2\pi\hbar)^3$. The kinetic equation for d electrons has a similar form.

The angle α between the vectors $\mathbf{p}$ and $\mathbf{E}$, the angle α' between the vectors $\mathbf{p}'$ and $\mathbf{E}$, and the angle θ between the vectors $\mathbf{p}$ and $\mathbf{p}'$ are related by the geometric formulas

$$\mathbf{p}'\mathbf{E} = p'E\cos\alpha' = p'E(\cos\alpha\cos\theta + \sin\alpha\sin\theta\cos\phi).$$

After integration over ϕ (the angle between the $(\mathbf{pp}')$ and $(\mathbf{pE})$ planes), we find

$$\mathbf{p}'\mathbf{E} = p'E\cos\alpha' = p'E\cos\alpha\cos\theta = \frac{p'}{p}\mathbf{pE}\cos\theta.$$

Owing to the δ function, the equality $p' = p$ is satisfied for the s–s scattering. We can eliminate the δ function by integration over ε'. As a result, we arrive at a set of kinetic equations

$$\eta_s(H_{ss} + G_{sd})\tau_s - \eta_d H_{sd}\tau_d = \eta_s, \quad (7)$$

$$\eta_s H_{ds}\tau_s - \eta_d(H_{dd} + G_{ds})\tau_d = -\eta_d, \quad (8)$$

which relate the relaxation times τ_s and τ_d. The coefficients in Eqs. (7) and (8) are as follows:

$$H_{ss}(\varepsilon) = \int_s W^{ss}(1-\cos\theta)(2N_\mathbf{q}+1)\frac{V}{(2\pi\hbar)^3}\frac{2\pi m_s}{p}qdq,$$

$$H_{sd}(\varepsilon) = \int_d W^{sd}\frac{p'}{p}\cos\theta(2N_\mathbf{q}+1)\frac{V}{(2\pi\hbar)^3}\frac{2\pi m_d}{p}qdq,$$

$$G_{sd}(\varepsilon) = \int_d W^{sd}(2N_\mathbf{q}+1)\frac{V}{(2\pi\hbar)^3}\frac{2\pi m_d}{p}qdq,$$

$$H_{dd}(\varepsilon) = \int_d W^{dd}(1-\cos\theta)(2N_\mathbf{q}+1)\frac{V}{(2\pi\hbar)^3}\frac{2\pi m_d}{p'}qdq,$$

$$H_{ds}(\varepsilon) = \int_s W^{ds}\frac{p}{p'}\cos\theta(2N_\mathbf{q}+1)\frac{V}{(2\pi\hbar)^3}\frac{2\pi m_s}{p'}qdq,$$

$$G_{ds}(\varepsilon) = \int_s W^{ds}(2N_\mathbf{q}+1)\frac{V}{(2\pi\hbar)^3}\frac{2\pi m_s}{p'}qdq.$$

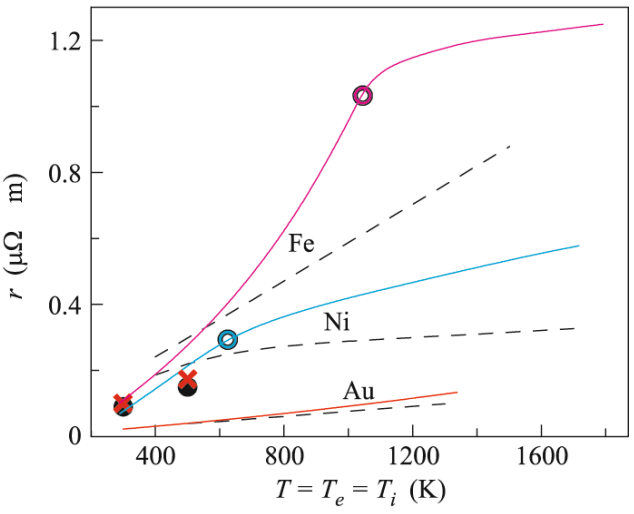

Fig. 2. (Dashed curves) Calculations by Eqs. (4)–(12) in comparison with (solid curves [15]) the experimental data.

The matrix elements W involved in these coefficients depend on the absolute value of momentum q.

A solution to the set of Eqs.(7) and (8) has the form

$$\tau_s(\varepsilon) = \frac{(m_s/m_d)H_{sd} + H_{dd} + G_{ds}}{(H_{ss} + G_{sd})(H_{dd} + G_{ds}) - H_{sd}H_{ds}}, \quad (9)$$

$$\tau_d(\varepsilon) = \frac{(m_s/m_d)H_{ds} + H_{ss} + G_{sd}}{(H_{ss} + G_{sd})(H_{dd} + G_{ds}) - H_{sd}H_{ds}}. \quad (10)$$

In Eqs. (9) and (10), we take into account that $\eta_d/\eta_s = m_s/m_d$. If the momentum of the electron is such that only the $s \longrightarrow s$ scattering is possible, the expression

$$\tau_s(\varepsilon) = 1/H_{ss} \quad (11)$$

is obtained instead of Eqs. (9) and (10).

To determine the relaxation times τ_s and τ_d, we performed the integration over ε' eliminating the δ function $\delta(\varepsilon' - \varepsilon)$. The requirement of a nonzero result of such integration imposes some limitations on the integration region in terms of the variables p and q. The most difficult and cumbersome stage of the calculations is just taking into account these geometric constraints. In this brief description, we omit this issue. The point is that the present paper is focused on the main effect, namely, the lowering of the e–i electrical resistance in transition metals with the growth of the temperature T_e. Concerning the double integration $\int\int dqdp$, we note that the integral $\int dq$ in the (pq) plane is calculated in order to determine the factors H and G in Eqs. (9)–(11).The integration over p arises in the calculations of the conductivity in terms of the relaxation time (see Eq. (12)).

Writing expressions for the current density, we determine the conductivities. The expression for the conductivity by means of s electrons has the form

$$\sigma_s = \frac{2}{3}\left(\frac{e}{m_s}\right)^2 \frac{4\pi}{(2\pi\hbar)^3}\int_p \left(-\frac{\partial f_{0s}}{\partial \varepsilon}\right)\tau_s(p)\frac{p^4 dp}{(2\pi\hbar)^3}, \quad (12)$$

where the derivative of the Fermi function f_{0s} is taken with respect to the energy $\varepsilon = \varepsilon_s + p^2/(2m_s)$ (see Eq. (3) and Fig. 1). The conductivity of d electrons $\sigma_d(T_e, T_i)$ is given by an expression similar to Eq. (12). Here, we should change subscripts ($s \longrightarrow d$), momenta ($p \longrightarrow p'$), and energy ($\varepsilon \longrightarrow \varepsilon'$). In the formula for the electrical conductivity σ_d, the Fermi function f_{0d} is differentiated with respect to the energy $\varepsilon' = \varepsilon_1 + (p')^2/(2m_d)$; see Eq. (3).

The total conductivity σ_{el-ph}, which is determined by the electron–phonon interaction, is $\sigma_{el-ph}(T_e, T_i) = \sigma_s + \sigma_d$. Figure 2 shows the temperature dependence of the electrical resistivity $r_{el-ph} = 1/\sigma_{el-ph}$ for the single-temperature (1T) case. Open circles on the experimental plots for nickel (Ni) and iron (Fe) mark the values of the Curie temperature (T_C = 628 K and 1041 K, respectively), below which these metals are in the ferromagnetic state. Formulas (4)–(12) are relevant to the phonon contribution to the electrical conductivity (the lattice part of the electrical resistivity r_{lat}) and disregard the additional scattering related to the magnetic fluctuations and to the excitation of spin waves (the magnetic contribution to the electrical resistivity r_{mag}). It is well known that $r_{lat} \propto T$ above the Debye temperature. The magnetic contribution is smaller but grows faster, $r_{mag} \propto T^3$ [14, 16]. Function $r_{mag}(T)$ attains the maximum at the Curie temperature, when the system undergoes the transition to the paramagnetic phase. Further on, it does not change, According to [17], $r_{mag}(T)$ equals 25 and 70% of $r_{lat}(T)$ at T = 300 and 500 K, respectively.

The above discussion concerning the temperature dependence of $r_{lat}(T)$ and $r_{mag}(T)$ makes it possible to separate the contribution r_{lat} from the measured total resistivity $r(T) = r_{lat} + r_{mag}$ [16, 17]. In [16, 18], sets of quantum calculations of $r_{lat}(T)$ were performed for the fcc lattice of iron with the Kubo–Greenwood formula [16] and for the bcc and hcp lattices of iron with the Eliashberg spectral functions [18]. In Eqs.(4)–(12), the crystal is approximated by an isotropic elastic medium. The calculations in [16, 18] were performed for temperatures up to 500 K with the most advanced currently existing techniques and the most powerful present-day computational resources. The data for T = 300 and 500 K reported in [16] and [18] are shown in Fig. 2 by the filled circles and skewed crosses, respectively. We can see that the data of [16, 18] agree well with our calculations by Eqs.(4)–(12) for iron in absolute value and slope. In the case of gold, the agree-

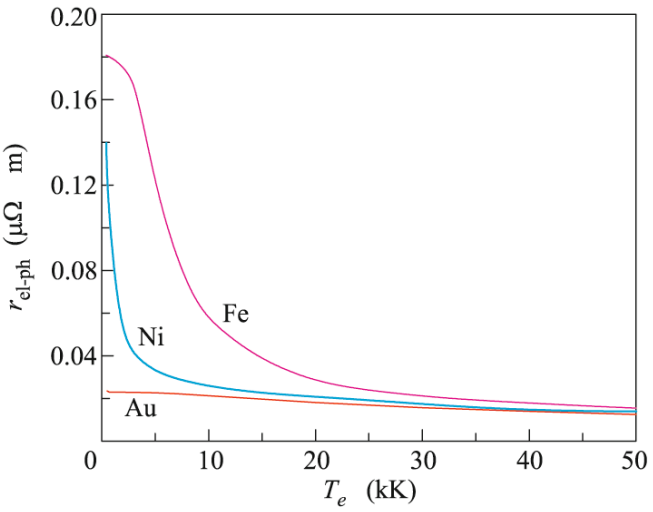

Fig. 3. Anomalous lowering of the electrical resistivity $r_{el-ph}(T_e, T_i = 300\ \text{K})$ with the growth of the electron temperature T_e for the case of *d* metals with the edge of the *d* band ε_2 (see Fig. 1) located above the Fermi level $\mu(T_e = 0)$.

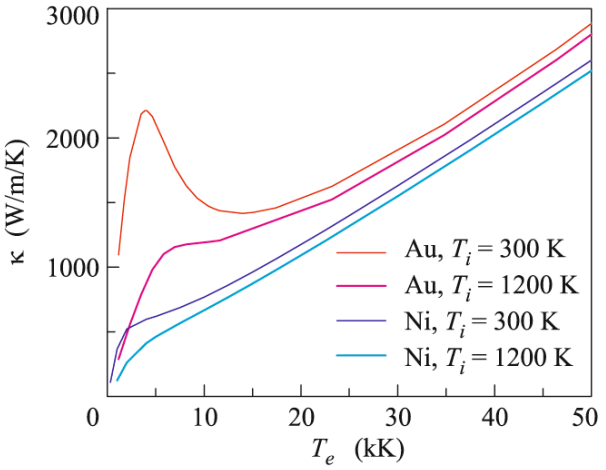

Fig. 4. Two-temperature thermal conductivities of nickel ($\varepsilon_2 > \mu(T_e = 0)$) and gold ($\varepsilon_2 < \mu(0)$).

ment of our calculations by Eqs.(4)–(12) with the experimental data is quite good.

The aforementioned calculations [16, 18] deal with the single-temperature situation. The first calculations [19, 20] for the two-temperature case ($T_e \gg T_i$) in a simple metal (aluminum) have recently been performed on the basis of the density functional method. The obtained results agree well with our semianalytical model [2, 3]. The calculations of the transport characteristics of metals with a complicated electron spectrum (e.g., nickel) using the density functional method are difficult and have not yet been carried out.

The aim of our calculations by Eqs.(4)–(12) is the description of the effect of the electron excitation on the electron–phonon interaction. The dependence of the lattice part of the electrical resistance $r_{el-ph}(T_e, T_i)$ on the electron temperature T_e at the ion temperature $T_i = 300$ K is shown in Fig. 3. In the case of nickel and iron, we see that the *e–i* interaction becomes weaker with the growth of the temperature T_e. Platinum exhibits a behavior similar to that of nickel. An appreciable difference in the electrical resistivity of nickel and iron (at room temperature), on one hand, and gold, on the other hand (see Figs. 2 and 3), characterizes the effect noticed by Mott [13, 14]. As was mentioned above, the increase in the electrical resistivity is caused by the presence of empty states in the *d* band. From Fig. 3, it follows that this effect is gradually reduced and vanishes when the temperature T_e becomes higher than the energy ε_2 ($\varepsilon_2 = 0.17$ eV for Ni and 1.4 eV for Fe). The qualitative explanation of the mechanisms underlying such a surprising behavior is given in Fig. 1. Note that, at rather high values of T_e, the electrical resistivity r_{el-ph} of the metals with different electron spectra turns out to be nearly the same.

Thus, in the case of the metals with $\varepsilon_2 > \mu(0)$, approximation (2) does not work well. Figure 4 shows the results for the thermal conductivity calculated taking into account the dependence of $\nu_{ei}(T_e, T_i)$ on two temperatures. This correction is not essential for the metals with $\varepsilon_2 < \mu(0)$ (e.g., for Al and Au). As we can see (Fig. 4), at high energies of the electron excitations, nickel and gold exhibit nearly the same values of the thermal conductivity. At the same time, under single-temperature conditions at temperatures above the Debye temperature but below the melting point, their values of the thermal conductivity significantly differ from each other: about 100 W/m/K for Ni and about 300 W/m/K for Au.

In conclusion, the coefficient κ has been calculated analytically for the first time involving both the electron–electron (*e–e*) and electron–ion (*e–i*) processes. Earlier, the *e–i* contribution was determined from experimental data [2–7]. For the transition metals, it has been found that the excitation of electrons significantly reduces the *e–i* contribution.

This work was supported by the Russian Foundation for Basic Research, project no. 11-08-01116-a.

REFERENCES

1. S. I. Anisimov, B. L. Kapeliovich, and T. L. Perel'man, Sov. Phys. JETP **39**, 375 (1974).
2. N. Inogamov and Yu. Petrov, J. Exp. Theor. Phys. **110**, 446 (2010).
3. Yu. V. Petrov, N. A. Inogamov, and K. P. Migdal, JETP Lett. **97**, 20 (2013).
4. M. B. Agranat, N. E. Andreev, S. I. Ashitkov, et al., JETP Lett. **85**, 271 (2007).

5. S. G. Bezhanov, A. P. Kanavin, and S. A. Uryupin, Quantum Electron. **41**, 447 (2011).
6. P. A. Loboda, N. A. Smirnov, A. A. Shadrin, et al., High Energy Dens. Phys. **7**, 361 (2011).
7. S. G. Bezhanov, A. P. Kanavin, and S. A. Uryupin, Opt. Spectrosc. **114**, 384 (2013).
8. V. Recoules, J. Clerouin, G. Zerah, et al., Phys. Rev. Lett. **96**, 055503 (2006).
9. V. V. Stegailov, Contrib. Plasma Phys. **50**, 31 (2010).
10. C. W. Siders, A. Cavalleri, K. Sokolowski-Tinten, et al., Science **286**, 1340 (1999).
11. D. Medvedev and Yu. Petrov, J. Exp. Theor. Phys. **88**, 128 (1999).
12. G. E. Norman, S. V. Starikov, and V. V. Stegailov, J. Exp. Theor. Phys. **114**, 792 (2012).
13. N. F. Mott, Proc. R. Soc. London A **153**, 699 (1936).
14. A. H. Wilson, Proc. R. Soc. London A **167**, 580 (1938).
15. G. Pottlacher, *High Temperature Thermophysical Properties of 22 Pure Metals* (Keiper, 2010).
16. D. Alfe, M. Pozzo, and M. P. Desjarlais, Phys. Rev. B **85**, 024102 (2012).
17. N. G. Baecklund, J. Phys. Chem. Solids **20**, 1 (1961).
18. X. Sha and R. Cohen, J. Phys.: Condens. Matter **23**, 075401 (2011).
19. M. E. Povarnitsyn, N. E. Andreev, E. M. Apfelbaum, et al., Appl. Surf. Sci. **258**, 9480 (2012).
20. G. E. Norman, S. V. Starikov, V. V. Stegailov, et al., Contrib. Plas. Phys. **53**, 129 (2013).

Translated by K. Kugel